

Nitriding Effects of Ammonia Flames on Iron-Base Metal Walls

Wang D^a, Lee M^a, Suzuki Y^{a*}

^aDepartment of Mechanical Engineering, The University of Tokyo, 7-3-1 Hongo, Bunkyo-ku, Tokyo 113-8656, Japan

Abstract

Effects of a $\text{NH}_3/\text{O}_2/\text{N}_2$ premixed flame/non-ignited mixture on iron-based metal walls have been investigated experimentally. A premixed $\text{NH}_3/\text{O}_2/\text{N}_2$ flame or non-ignited mixture formed by a quartz tube burner impinged on a disc-shaped metal test plate, of which the temperature was kept at 550 °C by an infrared lamp heater. As materials for the test plate, SACM645, SUS304, and SUS310S, which are widely used as industrial steels, were examined. After being exposed to either the $\text{NH}_3/\text{O}_2/\text{N}_2$ flame or non-ignited mixture for 5 hours, the surface hardness was measured by using a nano indenter. Distributions of nitrogen atoms diffused into the metal wall were measured by means of an Electron Probe Micro Analyzer (EPMA) and Secondary Ion Mass Spectrometry (SIMS). In addition, spatial distributions of the NH_3 concentration in the $\text{NH}_3/\text{O}_2/\text{N}_2$ flame and non-ignited mixture were measured by employing a two-photon absorption laser-induced fluorescence (TALIF) technique. It was found that the surface hardness of the test plates increased significantly after being exposed to the $\text{NH}_3/\text{O}_2/\text{N}_2$ flame/non-ignited mixture. The distributions of surface hardness and nitrogen atom concentration show that nitriding occurred by the present $\text{NH}_3/\text{O}_2/\text{N}_2$ flame/non-ignited mixture with the equivalent level of the conventional gas nitriding method. Moreover, it is also found that NH_3 concentration in the vicinity of the wall plays an important role in the surface hardness increase, and a wider distribution of NH_3 can result in a broader surface hardness distribution.

© 2022 The Authors. Published by Cardiff University Press.
Selection and/or peer-review under responsibility of Cardiff University

Received: 8th Jan 23; Accepted: 31st Mar 23; Published: 04th July 23

Keywords: Ammonia combustion, Nitriding, Surface hardness, Nitrogen atom concentration, Two-photon absorption laser-induced fluorescence (TALIF).

Introduction

In the past few decades, efforts have been made to reduce CO_2 emissions to slow down the progress of global warming. Combustion of fossil fuels has been the main source of CO_2 emissions. Therefore, developments of decarbonized fuels and improvements in combustion efficiencies are crucial. Hydrogen (H_2) has attracted attention in recent years because it can be produced from the electrolysis of water using renewable energy sources, and its carbon emission through the combustion process is zero. However, because the boiling temperature of hydrogen is as low as -253 °C, its transportation and storage are key challenges in hydrogen energy development. In such a context, ammonia (NH_3) has alternatively attracted attention as a promising hydrogen carrier. NH_3 has already been used in various industries, and accordingly, technologies for its production, transportation and storage are mature. In addition, despite its low combustibility, its utilization as a fuel through direct combustion has been tested in the fields of industrial furnaces [1] and gas turbines [2].

The combustion characteristics of NH_3 have been widely investigated, mainly focusing on its burning velocity and NO_x formation. Hayakawa et al. [3] and Takizawa et al. [4] reported that the laminar burning velocity of NH_3 /air premixed flames is around 7 cm/s, which is an order of magnitude lower when compared to hydrocarbon fuels. Hayakawa et al. [5] employed strain-stabilized ammonia/air premixed flames in a stagnation flow to investigate the product gas, and reported that the mole fractions of NO can be minimized under slightly-rich conditions, which corresponds to the equivalence ratio of 1.06.

In addition, detailed kinetic models for predicting ammonia reaction pathways have also been developed for better understanding of ammonia oxidation and pyrolysis. Okafor et al. [6] reported that the formation of NO is overestimated by GRI-Mech 3.0 [7], and modified the reaction between NH and H_2O . Nakamura et al. [8] reported the importance of the N_2H_x chemistry in the kinetic model at temperature ranges below 1027 °C and added the pyrolysis reaction. Recent reviews on combustion characteristics of NH_3 flames and modeling of their reaction pathways can be found in Refs. [9, 10].

* Corresponding author. Tel.: +81-3-5841-6411. E-mail address: ysuzuki@mesl.t.u-tokyo.ac.jp
<https://doi.org/10.18573/jae.8> Published under CC BY-NC-ND license. This license allows reusers to copy and distribute the material in any medium or format in unadapted form only, for noncommercial purposes only, and only so long as attribution is given to the creator.

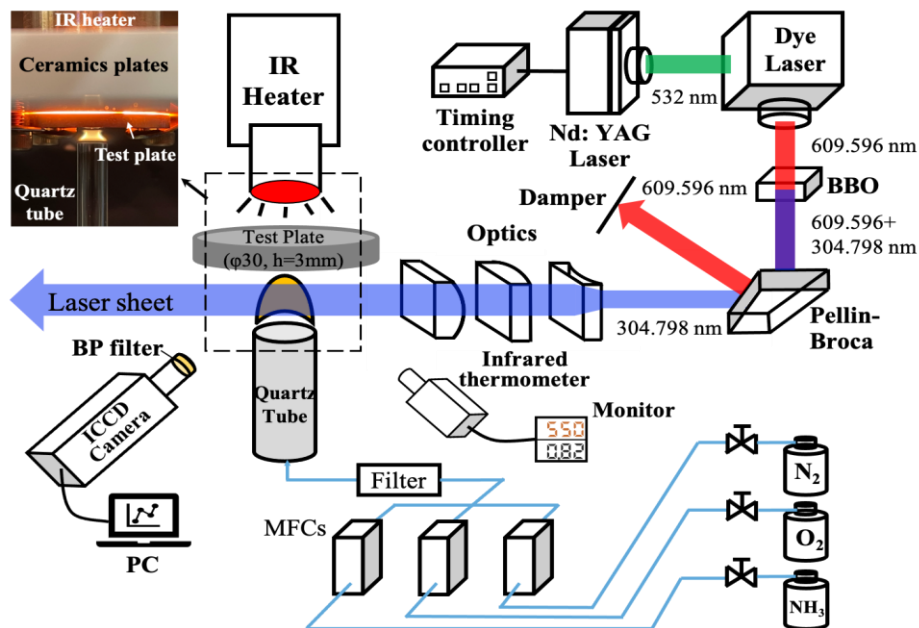


Fig. 1. Schematic of the ammonia combustion experimental setup and NH_3 -TALIF optical diagnostic system.

When flames exist in the vicinity of a wall, flame structures will be modified due to flame-to-wall interactions. In our previous studies, the wall chemical effects on radical pools in premixed flames such as a methane flame [11], dimethyl ether (DME) weak flame [12], nitrogen-diluted H_2 flame [13], and oxy-DME cool flame [14] have been investigated by employing a Planar Laser-Induced Fluorescence (PLIF) technique. These results show that the flame structures are significantly affected by the wall depending on its surface material.

When ammonia is employed as a fuel in industrial scenes, interactions between combustor walls and flames/non-ignited mixtures must be considered. While ammonia flames are affected by the metal wall surface, the metal wall surfaces themselves will also be influenced by ammonia flames/non-ignited mixtures. For instance, nitrogen atoms generated by the decomposition of ammonia on the surface can diffuse into the wall material and bond with metal atoms, such as Fe and Cr, leading to surface modification. This phenomenon is known as nitriding. This is a heat treatment aiming to improve the surface hardness of metal by diffusing nitrogen atoms to the surface, leading to the formation of nitrides. Nevertheless, “undesirable” nitriding can result in the surface hardness increase, making the material fragile [15], which is not preferable for its use as a combustor wall. Additionally, brittle and insufficiently protective nitride layers can be formed under an insufficient nitrogen diffusion condition, which will reduce the corrosion resistance to aqueous environments [16]. Tseng et al. [17] have reported that nitrogen atoms diffusing into iron-

based wall surfaces can generate Fe_3Nx , which can enhance the surface reactivity to ammonia. In general, austenitic stainless steels, such as SUS304 and SUS310S, are difficult to nitride without the prior pickling process due to the existence of passive films on their surface, while Sueyoshi et al. [18, 19] reported that SUS304 can possibly be nitrated due to the change of surface components after being preheated in air. Although gas nitriding has been widely studied as an industrial process, there is still a lack of knowledge on nitriding by NH_3 flames. Therefore, further quantitative investigation of the effect of NH_3 flames on metal walls is required.

The objective of the present study is to elucidate the effects of $\text{NH}_3/\text{O}_2/\text{N}_2$ flames and non-ignited mixtures on heated metal walls. SACM645, SUS304, and SUS310S were chosen as the wall materials. After exposure to a NH_3 flame/non-ignited mixture, the surface hardness was measured by using a nano indenter. In addition, distributions of nitrogen atom concentration in the plate were measured quantitatively. Furthermore, in situ measurements of the NH_3 spatial distribution were conducted by employing a Two-photon Absorption Laser-Induced Fluorescence (TALIF) technique to investigate the effects of the NH_3 distribution on the surface hardness and nitrogen atom concentration.

Materials and Methods

Exposure of metal walls to a $\text{NH}_3/\text{O}_2/\text{N}_2$ flame/non-ignited mixture

An experimental setup built in the present study is shown in Fig. 1. An $\text{NH}_3/\text{O}_2/\text{N}_2$ premixed jet flow was issued from a quartz tube with an inner diameter

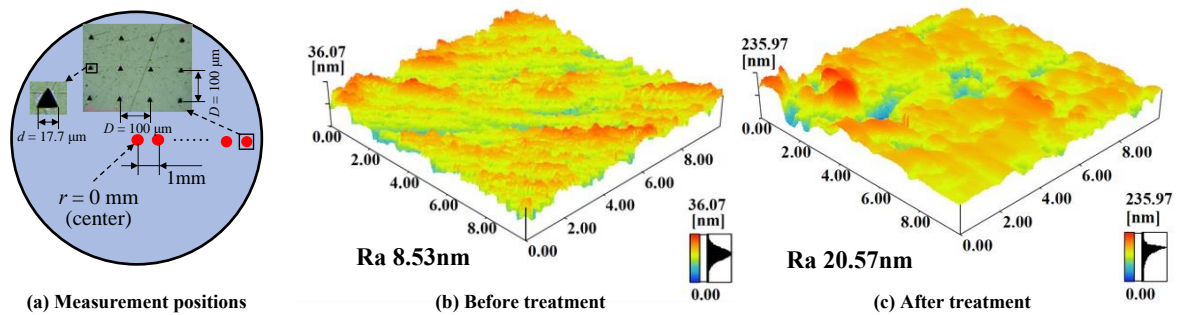


Fig. 2. Measurement positions (a) and surface roughness of SACM645 before (b) and after (c) the exposure to the $\text{NH}_3/\text{O}_2/\text{N}_2$ flame measured by the AFM.

of 4 mm and an outer diameter of 6 mm. Each gas was supplied from an individual gas cylinder and their flow rate was individually regulated by a mass flow controller (MFC, Model 3660, KOFLOC). The mixture impinged on a disc-shaped metal test plate ($\phi 30 \text{ mm} \times 3 \text{ mm}$), which was fixed under a high-temperature-tolerant ceramic substrate. The surface temperature of the metal plate was monitored at the position 14 mm away from the center of the test plate by using a radiation thermometer and was maintained at $550 \text{ }^\circ\text{C}$ using an infrared lamp heater (GVL298, THERMO RIKO) through a 25 mm-diameter center hole in the ceramic substrate. Note that a typical temperature used for gaseous nitriding is around $550 \text{ }^\circ\text{C}$ [20]. The distance between the tip of the tube nozzle and the surface of the test plate was adjusted using a z-axis stage. In the present study, it was fixed at 3.6 mm. Experiments were conducted under oxygen-enriched conditions to enhance the combustibility of NH_3 flames. The oxygen concentration (Ω), which is defined as the oxygen mole fraction in a mixture of oxygen and nitrogen, was kept at 0.4 (note that air gives $\Omega = 0.21$). The equivalence ratio and bulk mean velocity were 1.1 and 53 cm/s, respectively.

In addition to SACM645 (aluminum-chromium-molybdenum steel), which is commonly used as a nitriding steel, SUS304 and SUS310S (austenitic stainless steel) were selected as materials for the test plates. The chemical compositions of each material are shown in Table 1 [21, 22, 23].

Table 1. Chemical compositions of test plates (mass %).

	Cr	Al	C	Mn	Ni
SACM645	1.50	0.95	0.46	0.37	-
SUS304	18.28	-	0.06	0.89	8.54
SUS310S	25.00	-	0.08	2.00	20.00

Measurement of surface hardness

In order to minimize the unwanted effect of surface roughness on the surface hardness measurement, surfaces of the test plates were mirror-polished

before the NH_3 exposure. They were subjected to solution treatment process at $1025 \text{ }^\circ\text{C}$ in a vacuum furnace in order to remove the effects of work hardening that occurred due to polishing. Surface hardness distributions were measured by using a nano-indenter (ENT-NEXUS, ELIONIX). Figure 2a shows the measurement positions, which were selected at the center of the test plate and moved in the radial direction with 1 mm intervals. At each position, 25 measuring points were made by a 200 mN load with a spacing of $100 \text{ } \mu\text{m}$ to avoid interference among the measurement points. The indentations appear as black triangles with a length of $17.7 \text{ } \mu\text{m}$ as shown in Fig. 2a. Mean values among the 25 data points were used as the surface hardness. After exposure to the $\text{NH}_3/\text{O}_2/\text{N}_2$ flame/non-ignited mixture, wet polishing was also performed for 5 minutes by using a diamond slurry with an average grain size of $0.125 \text{ } \mu\text{m}$. The surface roughness was measured using an Atomic Force Microscope (AFM). As shown in Fig. 2b and 2c, the mean surface roughness before and after being exposed to the flame were respectively 8.53 nm and 20.57 nm in the scanned area of $10 \text{ } \mu\text{m} \times 10 \text{ } \mu\text{m}$, indicating that sufficiently smooth surfaces were obtained. The surface hardness was calculated by the load-

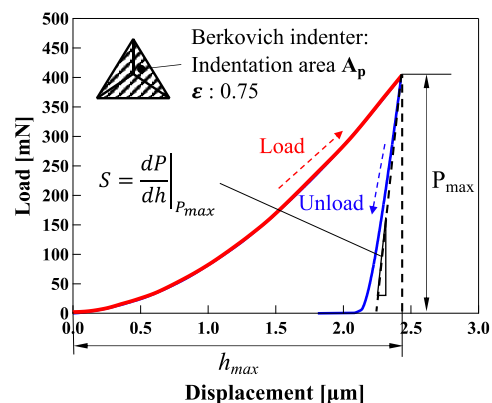


Fig. 3. Load-displacement curve from nano-indenter for calculating surface hardness.

displacement curve shown in Fig. 3. The red and blue lines represent the load and unload process of the indenter, respectively. The surface area of indentation A_p is used to calculate the Vickers hardness HV from the following equation,

$$HV = 0.0945 \times \frac{P_{max}}{A_p}, \quad (1)$$

where P_{max} is the maximum load. A_p is calculated from both the maximum contact depth h_{max} and stiffness S as follows,

$$A_p = 24.56 \times \left(h_{max} - \frac{P_{max}}{S} \varepsilon \right)^2. \quad (2)$$

where ε is a constant depending on the indenter type, with $\varepsilon = 0.75$ when the Berkovich indenter is used.

Measurements of nitrogen atom concentration

Concentrations of the nitrogen atoms diffused into the metal plate were measured after being exposed to the $NH_3/O_2/N_2$ flame/non-ignited mixture. The test plate was sliced by using a diamond wire saw (CS-203, Hitachi) and the cross sections were mirror-polished to identify the nitride layer. Distributions in the radial direction on the surface and in the depth direction at the center axis were measured by using a Dynamics SIMS (PHI ADEPT-1010, ULVAC-PHI) and an Electron Probe Micro Analyzer (EPMA - JXA-iSP100, JEOL), respectively.

NH_3 -TALIF

Spatial distributions of NH_3 concentration were measured by using the Two-photon Absorption Laser Induced Fluorescence (TALIF) technique [13, 24, 25, 26]. Following the study of Brackmann et al. [27], the excitation of the $C' \leftarrow X$ transition at 304.798 nm and fluorescence in the 568 nm $C \rightarrow A$ band were used for the NH_3 -TALIF measurement. As shown in Fig. 1, the NH_3 -TALIF system consists

of a Nd:YAG laser (LS2147, Lotis TII), a tunable dye laser (LiopStar-E&LSEH, Liop-Tec) with a dye mixture of sulforhodamine 640. The dye laser was pumped by the second harmonic (532 nm) of 10 Hz nanosecond Nd:YAG laser to generate a 609.596 nm laser beam. It was then frequency-doubled by a beta-barium borate (BBO) crystal for the second harmonic generation (SHG) to yield 304.798 nm. A combined laser beam of 609.596 nm and 304.798 nm was separated by a Pellin Broca prism. Three cylindrical lenses were used to form a laser sheet with a height of 6 mm. The laser was aligned to pass between the nozzle outlet and the wall surface. The fluorescence of NH_3 molecules was recorded by a Gen III ICCD camera (iStar 312T, Andor) with a band-pass filter centered at 568 nm (HWFHM: 10 nm). The measurement was conducted after exposing the test plate to the flame/non-ignited mixture for 5 hours. 500 single-shot images were taken and ensemble-averaged. The background level was captured and subtracted from the obtained image. The spatial intensity variation in the laser sheet was compensated with pure NH_3 fed into a quartz cell. The dependence of the NH_3 -TALIF intensity on the laser energy density was examined (not shown). The results show a quadratic correlation in the range of 0.54-0.86 mJ/pulse, confirming that the effect of photolytic interference is negligible in the present measurement.

Results and discussions

Surface modification

Figure 4 shows the optical micrographs of the SACM645 and SUS304 test plates after being exposed to the $NH_3/O_2/N_2$ flame at 550 °C for 5 hours. Both surfaces have been significantly modified after the exposure, particularly near the center. While dependence on the radial position is

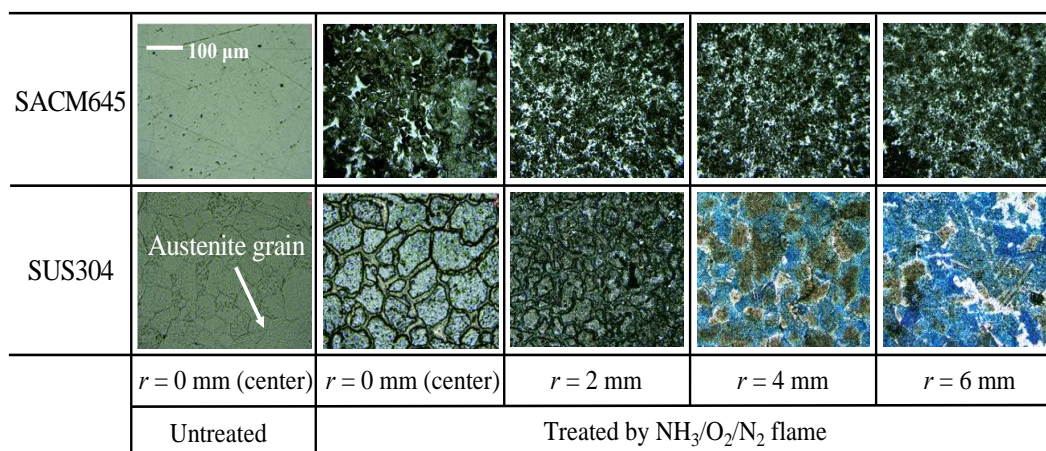


Fig. 4. Optical micrographs of the SACM645 and SUS304 test plate surfaces after being exposed to the $NH_3/O_2/N_2$ flame at 550 °C for 5h. (Austenite is seen as the polygonal texture on the surface of untreated SUS304).

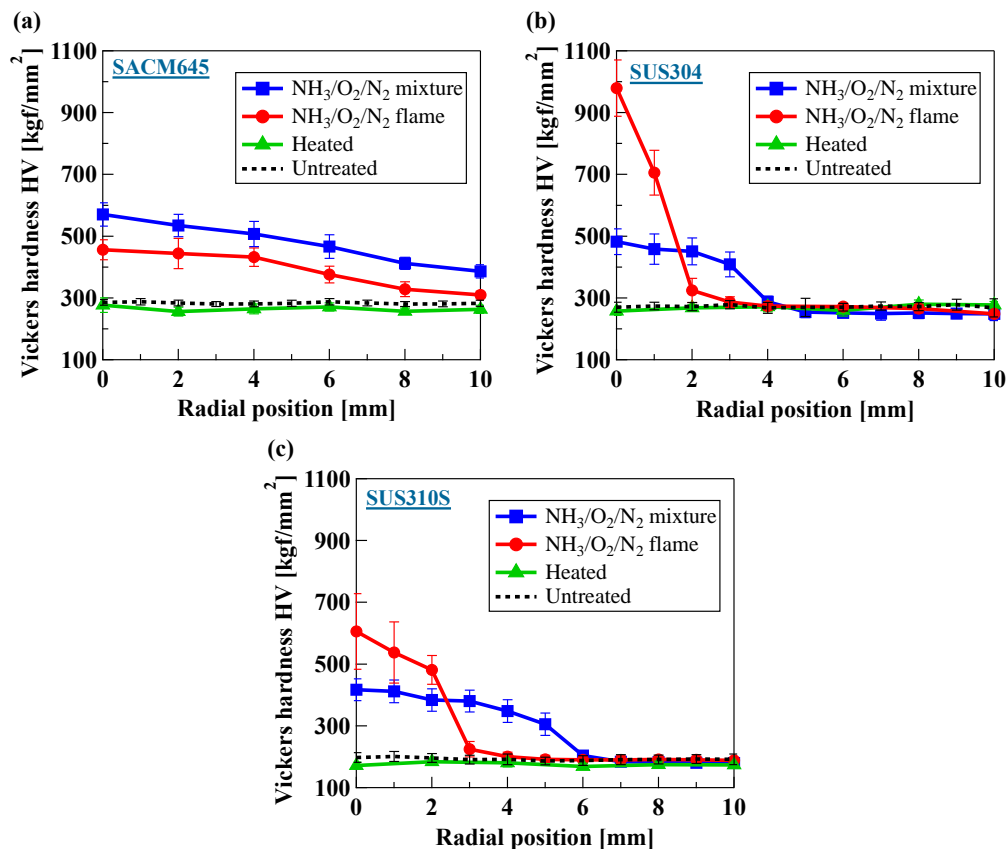


Fig. 5. Radial distributions of surface hardness of the SACM645, SUS304 and SUS310S test plates after being exposed to the NH₃/O₂/N₂ flame/non-ignited mixture at 550 °C for 5h.

hardly observed on the SACM645 test plate, the surface modification on the SUS304 test plate shows different behaviors depending on the radial position. In the latter case, the precipitates consisting of chromium and iron nitrides are observed at $r \leq 2$ mm. They cover the austenite, of which the microstructure is shown in the untreated case of SUS304, implying nitriding can occur regardless of the grain interiors or austenite boundaries. This result shows a similar trend with the surface treated by gas nitriding for 20 hours [28]. It is noticeable that the oxidation layers (blue regions) together with some precipitates are also confirmed at $r \geq 4$ mm, indicating nitriding does not fully proceed at further radial positions.

Effect on the surface hardness

Figure 5 shows the surface hardness distributions of the SACM645, SUS304 and SUS310S test plates after being exposed to the NH₃/O₂/N₂ flame or non-ignited mixture. They are also compared with the result after heating the samples at 550 °C in air for 5 hours. For the SACM645 test plate, the surface hardness is found to be 284 kgf/mm² before exposure, which is in good agreement with the

literature value [29]. After heating at 550 °C in air, the surface hardness slightly decreases to 277 kgf/mm² at $r = 0$ mm due to the annealing effect. On the other hand, when the test plate is exposed to NH₃/O₂/N₂ flame and mixture for 5 hours, the surface hardness at $r = 0$ mm increases to approximately 456 kgf/mm² and 570 kgf/mm², respectively, indicating that nitriding occurred. In previous studies, it was reported that the hardness of SACM645 increased to 820 kgf/mm² as a result of gas nitriding in a pure NH₃ atmosphere at 580 °C for 20 hours [30]. In the present study, the increase in the surface hardness is slightly lower than that in the gas nitriding case, which is attributed to the shorter exposure time. However, the effects of nitriding on the surface hardness induced by the NH₃/O₂/N₂ flame and non-ignited mixture is confirmed. In addition, the surface hardness decreases as the radial distance increases, and the effect of nitriding almost disappears at $r = 10$ mm. Furthermore, effects of the NH₃/O₂/N₂ non-ignited mixture on the surface hardness are more significant than that of the flame. These results are caused by the differences in the NH₃ concentration in the vicinity of wall, which will be discussed later. The effects of NH₃/O₂/N₂ flame

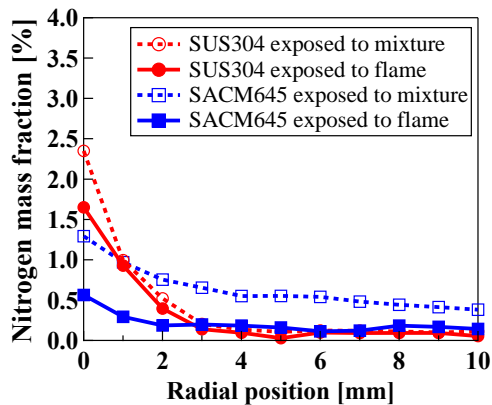


Fig. 6. Radial distributions of nitrogen atom concentrations on the SACM645 and SUS304 surface after being exposed to the $\text{NH}_3/\text{O}_2/\text{N}_2$ flame/non-ignited mixture at 550 °C for 5 hours.

and non-ignited mixture on the surface hardness distributions of stainless steels are highly different from those of SACM645 as shown in Figs. 5b and c. The initial surface hardness is 272 kgf/mm² and 193 kgf/mm² for SUS304 and SUS301S, respectively. The effect of heating on the surface hardness hardly appears for the stainless steel test plates. On the other hand, after being exposed to the flame or non-ignited mixture, the surface hardness at $r = 0$ mm increases to 979 kgf/mm² and 482 kgf/mm² for SUS304, and 606 kgf/mm² and 417 kgf/mm² for SUS310S, respectively. These results indicate that nitriding induced by NH_3 flames also occurs on the surfaces of stainless steel. After being exposed to the NH_3 flame, SUS304 and SUS310S show similar trends in the surface hardness distribution, that the areas of nitriding are localized near the center ($r \leq 4$ mm for the flame and $r \leq 6$ mm for the non-ignited mixture case), and it hardly proceeds at further radial positions. The surface hardness distribution of SUS304 is in good accordance with the result shown in Fig. 4, where the nitriding regions are only observed near the center, while the oxidation layers are observed away from the center. Since the surface hardness distributions of SUS304 and SUS310S show similar trends, further investigations are focused on SUS304 and SACM645.

Diffusion of nitrogen atoms

Figure 6 shows radial distributions of nitrogen atom concentrations on the SACM645 and SUS304 surfaces after being exposed to the $\text{NH}_3/\text{O}_2/\text{N}_2$ flame/non-ignited mixture. The mass fractions of nitrogen reach 1.3% and 2.4% at the center of the SACM645 and SUS304 plates when exposed to the non-ignited mixture, while they increase to 0.6%

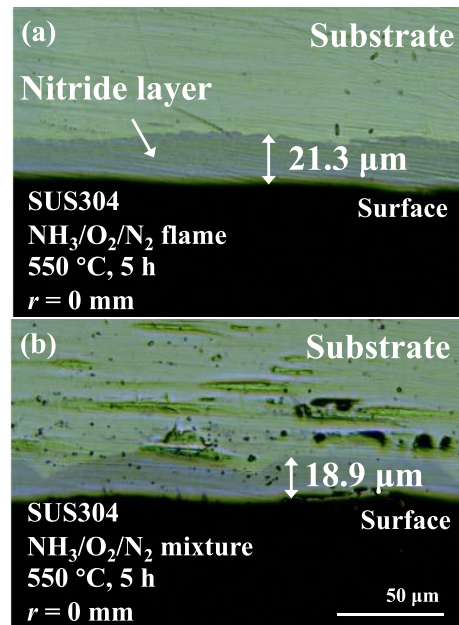


Fig. 7. Cross-sectional microstructures at $r = 0$ mm of SUS304 after being exposed to the (a) $\text{NH}_3/\text{O}_2/\text{N}_2$ flame and (b) non-ignited mixture.

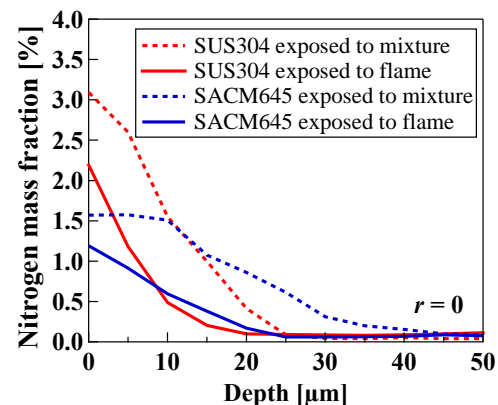


Fig. 8. Nitrogen atom distributions of SACM645 and SUS304 at the center ($r = 0$ mm) in the depth direction after being exposed to the $\text{NH}_3/\text{O}_2/\text{N}_2$ flame/non-ignited mixture at 550 °C for 5 hours.

Note that the values at the surface (vertical intercepts) are slightly different from the result shown in Fig. 6, attributed to the positioning accuracy of the measurement points at each surface.

and 1.7% for those exposed to the flame, respectively. Nitrogen mass fraction gradually decreases with increasing the radial direction and becomes almost zero at $r > 4$ mm for SUS304, while, for SACM645, it distributes evenly at $r < 10$ mm. These results are also in good accordance with the distribution of surface hardness shown in Figs. 5a and b, indicating that the increase in the surface hardness is caused by the diffusion of nitrogen atoms. However, it is worth noting that the nitrogen

atom concentration at the SUS304 surface ($r = 0$) is relatively high while the increase in surface hardness is lower after being exposed to the $\text{NH}_3/\text{O}_2/\text{N}_2$ non-ignited mixture, showing that the increment of surface hardness is not necessarily a unique function of the nitrogen atom concentration. On the other hand, the weakened nitriding effect away from the center axis of the SUS304 surface may be attributed to lower NH_3 concentration which will be discussed in the following section. The nitrogen mass fraction on the SACM645 surface is approximately half of the value achieved by the conventional gas nitriding performed under pure NH_3 atmospheres at $580\text{ }^\circ\text{C}$ for 20 hours [30]. The discrepancy in the nitrogen mass fraction is attributed to the shorter exposure time. Nonetheless, it was confirmed that the equivalent level of the nitriding effect can be obtained through impingements of the $\text{NH}_3/\text{O}_2/\text{N}_2$ flame/non-ignited mixture. To better understand the effects of $\text{NH}_3/\text{O}_2/\text{N}_2$ flame/non-ignited mixture on the SUS304 surface, microstructures of the cross-section were observed as shown in Fig. 7. The nitride layers with a thickness of $21.3\text{ }\mu\text{m}$ and $18.9\text{ }\mu\text{m}$ can be observed clearly in the flame and non-ignited mixture cases, respectively. Note that the black dots are shadows on the cross-section surface caused by defects in the sample and incomplete polishing. Figure 8 shows the nitrogen atom distributions of SACM645 and SUS304 in the depth direction at $r = 0\text{ mm}$ after being exposed to the $\text{NH}_3/\text{O}_2/\text{N}_2$ flame/non-ignited mixture. For SACM645 exposed to the non-ignited mixture, the nitrogen atom diffuses as deep as $50\text{ }\mu\text{m}$, while the diffusion depth for SUS304 under the same condition is around $25\text{ }\mu\text{m}$, which is close to the nitride layer thickness

shown in Fig. 7. The nitride layer thickness of SACM645 is also slightly thicker than that of SUS304 after being exposed to the flame, which shows a similar trend to that exposed to the non-ignited mixture. Differences in the nitride layer thickness are believed to be caused by different diffusion speeds of nitrogen atoms in SACM645 and SUS304. The main phase of SACM645 is ferrite ($\alpha\text{-Fe}$) with body-centered cubic (BCC) structures while that of SUS304 is austenite ($\gamma\text{-Fe}$) with face-centered cubic (FCC) structures, in which the diffusion coefficient magnitude of nitrogen atoms is 0.0047 and $0.0034\text{ cm}^2/\text{s}$, respectively [31]. As a result, nitrogen atoms can diffuse deeper in the BCC structure if the exposure time is the same. On the other hand, the higher nitrogen atom concentration at $r = 0\text{ mm}$ in SUS304 has been observed for both the flame and non-ignited mixture cases, compared to SACM645. The phenomenon is attributed to the higher solubility of nitrogen atom in $\gamma\text{-Fe}$ (4.5 wt%) than that in $\alpha\text{-Fe}$ (0.1 wt%) [32].

Effects of NH_3 distribution on surface hardness

Two-dimensional NH_3 -TALIF measurements were performed to capture spatial distributions of NH_3 near the wall surface. Figure 9 shows the NH_3 distribution in the $\text{NH}_3/\text{O}_2/\text{N}_2$ flame/non-ignited mixture on the SACM645 and SUS304 surfaces; 0 mm and 3.6 mm at the axial position correspond to the wall surface and the location of the tube outlet, respectively. It is confirmed that NH_3 distributes widely in the non-ignited mixture, while it is hardly observed at the downstream side of the flame front. Differences in the NH_3 distributions should explain the difference in the surface hardness distribution

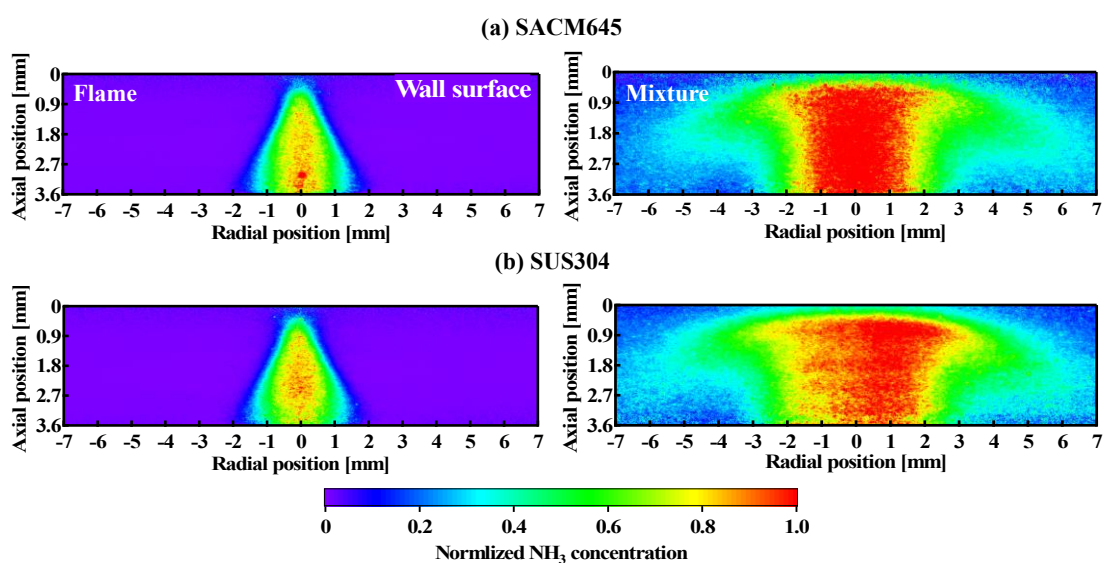


Fig. 9. 2-D distributions of NH_3 concentration in $\text{NH}_3/\text{O}_2/\text{N}_2$ flame (left column) and non-ignited mixture (right column) in the vicinity of the heated wall at $550\text{ }^\circ\text{C}$. (a) SACM645, and (b) SUS304 surfaces.

between the flame and non-ignited mixture cases shown in Fig. 5b, implying the NH_3 concentration affects the distribution of nitriding regions. In general, SUS304 is hard to be nitrided due to inherent passive films formed on its surface, while the heating process may modify their composition as reported by Sueyoshi et al. [18, 19]. Therefore, nitriding can possibly occur at all regions on the SUS304 surface, while the surface hardness increases only near the center after being exposed to the $\text{NH}_3/\text{O}_2/\text{N}_2$ flame or non-ignited mixture, where the NH_3 concentration is high. For the same reason, higher concentration and larger diffusion depth of nitrogen atoms are observed both in the SACM645 and SUS304 test plates after being exposed to the non-ignited mixture, if compared to those exposed to the flame. Although NH_3 plays a dominant role in nitriding, the higher surface hardness of SUS304 after being exposed to the flame at $r = 0$ mm is also confirmed with lower near-wall NH_3 concentration. This indicates that the increase in surface hardness does not only depend on the nitrogen atom concentration diffused into the material and the near-wall NH_3 concentration, but also on the characteristic composition of the material and its bonding condition with nitrogen atoms. Differences in the NH_3 distribution on different materials are barely noticeable for both flame and non-ignited mixture cases, indicating a similar wall chemical effect on iron-based metal materials. However, surface hardness distributions are different for each case as shown in Fig. 5. Therefore, it is considered that nitriding is mainly governed by the intrinsic characteristics of the materials.

Conclusions

In this study, effects of a $\text{NH}_3/\text{O}_2/\text{N}_2$ flame/non-ignited mixture on iron-based metal walls were quantitatively investigated. SACM645, SUS304 and SUS310S test plates heated to 550 °C were exposed to either a $\text{NH}_3/\text{O}_2/\text{N}_2$ premixed flame or non-ignited mixture for 5 hours. Distributions of surface hardness and nitrogen atoms were measured to examine the nitriding effect that occurred on the surface. Additionally, NH_3 distributions near the wall surface were also measured by employing NH_3 -TALIF to evaluate the effects of NH_3 concentration on surface hardness. The following conclusions have been derived.

1. Exposure to either $\text{NH}_3/\text{O}_2/\text{N}_2$ flames or non-ignited mixtures can cause a significant increase in the surface hardness resulting from nitriding. This confirms that exposures to the $\text{NH}_3/\text{O}_2/\text{N}_2$ flame/non-ignited mixture increase the surface hardness and nitrogen atom concentration to the equivalent level of conventional gas nitriding.

2. The radial distributions of the nitrogen atom on the SACM645 and SUS304 surface show good accordance with those of the surface hardness, while the distribution in the depth direction implies that nitrogen concentration may not determine the surface hardness directly on its own.
3. The nitrided region on the SUS304 surface is localized to $r \leq 4$ mm and $r \leq 6$ mm for the flame and non-ignited mixture cases, respectively. The NH_3 -TALIF results confirm that the distribution of the NH_3 concentration near the surface plays an essential role in nitriding.

Acknowledgments

The authors acknowledge Prof. Junichiro Shiomi and Dr. Bin Xu for their assistance in using a nano indenter. This work was supported by JSPS KAKENHI Grant Number 21H04539, NEDO Feasibility Study Program "Development of Carbon-neutral Industrial Furnace by Innovative Ammonia Combustion" funded by NEDO, Japan, and JST SICORP EIG CONCERT-Japan Grant Number JPMJSC21C1. A part of this work was supported by "Advanced Research Infrastructure for Materials and Nanotechnology in Japan (ARIM)" of MEXT Proposal Number JPMXP1222UT1011. M.L. was partially supported by the Paloma Environmental Technology Development Foundation.

Conflicts of Interest

The authors declare no conflict of interest. The funders had no role in the design of the study; in the collection, analyses, or interpretation of data; in the writing of the manuscript, or in the decision to publish the results.

References

1. Murai R, Omori R, Kano R, Tada Y, Higashino H, Nakatsuka N, Hayashi J, Akamatsu F, Iino K, Yamamoto Y. The radiative characteristics of $\text{NH}_3/\text{N}_2/\text{O}_2$ non-premixed flame on a 10 kW test furnace. *Energy Procedia*. 2017; 120: 325-332. DOI: <https://doi.org/10.1016/j.egypro.2017.07.232>.
2. Kurata O, Iki N, Inoue T, Matsunuma T, Tsujimura T, Furutani H, Kawano M, Arai K, Okafor EC, Hayakawa A, Kobayashi H. Development of a wide range-operable rich-lean low- NO_x combustor for NH_3 fuel gas-turbine power generation. *Proceedings of the Combustion Institute*. 2019; 37(4): 4587-4595. DOI: <https://doi.org/10.1016/j.proci.2018.09.012>.
3. Hayakawa A, Goto T, Mimoto R, Arakawa Y, Kudo T, Kobayashi H. Laminar burning velocity and Markstein length of ammonia/air premixed

- flames at various pressures. *Fuel*. 2015; 159(1): 98-106. DOI: <https://doi.org/10.1016/j.fuel.2015.06.070>.
4. Takizawa K, Takahashi A, Tokuhashi K, Kondo S, Sekiya A. Burning velocity measurements of nitrogen-containing compounds. *Journal of Hazardous Materials*. 2008; 155(1-2): 144-152. DOI: <https://doi.org/10.1016/j.jhazmat.2007.11.089>
5. Hayakawa A, Hirano Y, Okafor EC, Yamashita H, Kudo T, Kobayashi H. Experimental and numerical study of product gas characteristics of ammonia/air premixed laminar flames stabilized in a stagnation flow. *Proceedings of the Combustion Institute*. 2021; 38(2): 2409-2417. DOI: <https://doi.org/10.1016/j.proci.2020.07.030>.
6. Okafor EC, Naito Y, Colson S, Ichikawa A, Kudo T, Hayakawa A, Kobayashi H. Measurement and modelling of the laminar burning velocity of methane-ammonia-air flames at high pressures using a reduced reaction mechanism. *Combustion and Flame*. 2019; 204: 162-175. DOI: <https://doi.org/10.1016/j.combustflame.2019.03.008>.
7. Smith GP, Golden DM, Frenklach M, Moriarty NW, Eiteneer B, Goldenberg M, Bowman CT, Hanson RK, Song S, Gardiner WC, Lissianski VV, Qin Z. GRI-Mech 3.0, 2011. Available in: http://www.me.berkeley.edu/gri_mech/ (accessed 13th December 2022)
8. Nakamura H, Hasegawa S, Tezuka T. Kinetic modeling of ammonia/air weak flames in a micro flow reactor with a controlled temperature profile. *Combustion and Flame*. 2017; 185: 16-27. DOI: <https://doi.org/10.1016/j.combustflame.2017.06.021>.
9. Kobayashi H, Hayakawa A, Somaratne KDKA, Okafor EC. Science and technology of ammonia combustion. *Proceedings of the Combustion Institute*. 2019; 37(1): 109-133. DOI: <https://doi.org/10.1016/j.proci.2018.09.029>.
10. Elbaz AM, Wang S, Guiberti TF, Roberts WL. Review on the recent advances on ammonia combustion from the fundamentals to the applications. *Fuel Communications*. 2022; 10: 100053. DOI: <https://doi.org/10.1016/j.jfueco.2022.100053>
11. Saiki Y, Fan Y, Suzuki Y. Radical quenching of metal wall surface in a methane-air premixed flame. *Combustion and Flame*. 2015; 162(10): 4036-4045. DOI: <https://doi.org/10.1016/j.combustflame.2015.07.043>.
12. Wan S, Fan Y, Maruta K, Suzuki Y. Wall chemical effect of metal surfaces on DME/air cool flame in a micro flow reactor. *Proceedings of the Combustion Institute*. 2019; 37(4): 5655-5662. DOI: <https://doi.org/10.1016/j.proci.2018.05.165>.
13. Fan Y, Guo J, Lee M, Iki N, Suzuki Y. Quantitative evaluation of wall chemical effect in hydrogen flame using two-photon absorption LIF. *Proceedings of the Combustion Institute*. 2021; 38(2): 2361-2370. DOI: <https://doi.org/10.1016/j.proci.2020.06.021>.
14. Lee M, Fan Y, Ju Y, Suzuki Y. Ignition characteristics of premixed cool flames on a heated wall. *Combustion and Flame*. 2021; 231: 111476. DOI: <https://doi.org/10.1016/j.combustflame.2021.111476>.
15. Akhtar SS, Arif AFM, Yilbas B. Evaluation of gas nitriding process with in-process variation of nitriding potential for AISI H13 tool steel. *The International Journal of Advanced Manufacturing Technology*. 2010; 47: 687-698. DOI: <https://doi.org/10.1007/s00170-009-2215-4>.
16. Yakuwa H, Noguchi M. Lecture on fundamental aspects of high temperature corrosion and corrosion protection Part 6: Examples of carburization, nitridation and steam oxidation in high-temperature devices and countermeasures. *Ebara Engineering Review*. 2018; 256: 1-14.
17. Tseng JC, Gu D, Pistidda C, Horstmann C, Dornheim M, Ternieden J, Weidenthaler C. Tracking the active catalyst for iron-based ammonia decomposition by in situ synchrotron diffraction studies. *ChemCatChem*. 2018; 10(19): 4465-4472. DOI: <https://doi.org/10.1002/cctc.201800398>.
18. Sueyoshi H, Hamaishi K, Kadomatsu S, Shiomizu T, Ohzono Y. Effect of preheating in air on gas nitriding of SUS304. *Materials Transactions, JIM*. 1997; 38(2): 148-154. DOI: <https://doi.org/10.2320/matertrans1989.38.148>.
19. Sueyoshi H, Hamaishi K, Shiomizu T, Ohzono Y. Effect of preheating in air on gas nitriding of austenitic stainless steels. *Materials Transactions, JIM*. 1998; 39(8): 849-856. DOI: <https://doi.org/10.2320/matertrans1989.39.849>.
20. Lu J, Wang Q, Liu C, Zhang C, Chen D, Cui G. Cracking behavior of AISI 316L stainless steel powder by gas nitriding and its influence on spark plasma sintering. *Journal of Materials Research and Technology*. 2022; 20: 3796-3806. DOI: <https://doi.org/10.1016/j.jmrt.2022.08.163>.
21. Hirao M, Fuse T, Shirase K, Yasui T, Shiraga T, Ishikawa N. Improved machinability of nitriding steel (SACM 645). *Journal of Materials Processing Technology*. 1996; 62(4): 370-373. DOI: [https://doi.org/10.1016/S0924-0136\(96\)02437-5](https://doi.org/10.1016/S0924-0136(96)02437-5).
22. Shindo Y, Yamaguchi Y, Horiguchi K. Small punch testing for determining the cryogenic fracture properties of 304 and 316 austenitic stainless steels in a high magnetic field. *Cryogenics*. 2004; 44(11): 789-792. DOI: <https://doi.org/10.1016/j.cryogenics.2004.04.008>.

23. Dong Z, Wei Y, Xu Y. Predicting weld solidification cracks in multipass welds of SUS310 stainless steel. *Computational Materials Science*. 2006; 38(2): 459-466. DOI: <https://doi.org/10.1016/j.commatsci.2006.03.018>.
24. Aldén M, Edner H, Grafström P, Svanberg S. Two-photon excitation of atomic oxygen in a flame. *Optics Communications*. 1982; 42(4): 244-246. DOI: [https://doi.org/10.1016/0030-4018\(82\)90025-6](https://doi.org/10.1016/0030-4018(82)90025-6).
25. Uddi M, Jiang N, Mintusov E, Adamovich IV, Lempert WR. Atomic oxygen measurements in air and air/fuel nanosecond pulse discharges by two photon laser induced fluorescence. *Proceedings of the Combustion Institute*. 2009; 32(1): 929-936. DOI: <https://doi.org/10.1016/j.proci.2008.06.049>.
26. Fan Y, Guo J, Lee M, Iki N, Suzuki Y. Evaluation of wall chemical effect in hydrogen flame. *Proceedings of the Combustion Institute*. 2021; 38: 2361-2370. DOI: <https://doi.org/10.1016/j.proci.2020.06.021>.
27. Brackmann C, Hole O, Zhou B, Li ZS, Aldén M. Characterization of ammonia two-photon laser-induced fluorescence for gas-phase diagnostics. *Applied Physics B*. 2014; 115: 25-33. DOI: <https://doi.org/10.1007/s00340-013-5568-1>.
28. Sueyoshi H, Hamaishi K, Shiomizu T. Effect of processing condition on gas nitriding of austenitic stainless steels. *Materials Transactions, JIM*. 1999; 40(1): 13-19. DOI: <https://doi.org/10.2320/matertrans1989.40.13>.
29. Hirao M, Fuse T, Shirase K, Yasui T, Shiraga T, Ishikawa N. Improved machinability of nitriding steel (SACM 645). *Journal of Materials Processing Technology*. 1996; 62(4): 370-373. DOI: [https://doi.org/10.1016/S0924-0136\(96\)02437-5](https://doi.org/10.1016/S0924-0136(96)02437-5).
30. Ishikawa N, Shiraga T, Sato K, Ishiguro M, Kabasawa H, Kuwahara Y. Effects of nitriding temperature on gas nitriding property of steels for nitriding. *Tetsu-to-Hagane*. 1996; 82(2): 164-169. (in Japanese) DOI: https://doi.org/10.2355/tetsutohagane1955.82.2_164.
31. Askeland DR, Wright WJ. Atom and ion movements in materials. In Askeland DR., Wright WJ. (eds.) *The science and engineering of materials* (seventh edition). Boston: Cengage Learning; 2014. pp. 148-150.
32. Wriedt HA, Gokcen NA, Nafziger RH. The Fe-N (Iron-Nitrogen) system. *Bulletin of Alloy Phase Diagrams*. 1987; 8: 355-377. DOI: <https://doi.org/10.1007/BF02869273>.